J. Fluid Mech. (2007), *vol.* 592, *pp.* 393–411. © 2007 Cambridge University Press
doi:10.1017/S002211200700849X Printed in the United Kingdom

Hydrodynamically coupled rigid bodies

SUJIT NAIR AND EVA KANSO
University of Southern California, Los Angeles, CA 90089, USA

(Received 31 October 2006 and in revised form 6 August 2007)

This paper considers a finite number of rigid bodies moving in potential flow. The dynamics of the solid–fluid system is described in terms of the solid variables only using Kirchhoff potentials. The equations of motion are first derived for the problem of two submerged bodies where one is forced into periodic oscillations. The hydrodynamic coupling causes the free body to drift away from or towards the oscillating body. The method of multiple scales is used to separate the slow drift from the fast response. Interestingly, the free body, when attracted towards the forced one, starts to drift away after it reaches certain separation distance. This suggests that the hydrodynamic coupling helps in preventing collisions. The fluid's role in collision avoidance and motion coordination is examined further through examples. In particular, we show that a free body can coordinate its motion with that of its neighbours, which may be relevant to understanding the coordinated motion in fish schooling.

1. Introduction

This paper considers the motion of systems of solid bodies in potential flow. The primary motivation is to study the effect of the hydrodynamic coupling on the motion of the submerged solids and gain insight into the importance of this coupling in fish schooling.

Early efforts in developing mathematically sound models of swimming can be attributed to Gray, Childress, Lighthill, Taylor and Wu; see, e.g., Childress (1981), Lighthill (1975), Taylor (1952) and Wu (1971). Interest has re-emerged over the past few years in understanding the mechanics of fish swimming and thereby enable novel engineering applications such as the design of biologically inspired vehicles that move and steer by *shape changes* rather than by direct propulsion. For recent experimental studies of the shape kinematics of live fish and its interaction with the surrounding fluid, see, for example, Liao *et al.* (2003), Müller (2003), and Webb (1991). See also Kelly (1998) and Radford (2003) for their fundamental work on the mathematical formulation of aquatic locomotion using tools from geometric mechanics. In Kanso & Marsden (2005) and Kanso *et al.* (2005), we modelled the fish as an articulated body and formulated the equations governing its motion in potential flow. We showed under these idealized conditions, i.e. in the absence of a vortex shedding mechanism, that the articulated body can propel and steer itself by changing its shape only. The net locomotion in potential flow occurs due to the transfer of momentum between the solid and the fluid: starting from rest, the articulated body changes its shape by applying internal torques at its joints. The shape actuation sets the surrounding fluid into motion, and the coupling between the shape dynamics and the surrounding fluid causes a net locomotion of the solid. This result is important because it demonstrates that one could capture some features of aquatic locomotion using simple potential flow models with no shed vortices. Indeed, our models are close

in spirit to Lighthill's 'reactive' force theory for the swimming of elongated fish (e.g. Carangiform fish) at large Reynolds number, see Lighthill (1975). He argues that the added or virtual mass of fluid which acquires momentum through shape changes of the animal far exceeds the associated animal's mass and the 'resistive' forces due to boundary layer and vortex shedding; hence, the 'reactive' forces (proportional to the added mass) play a central role in the locomotion of these animals. It is exactly this (added mass) effect that we capture in the potential flow models.

In this paper, we study the hydrodynamic-coupling effects on the motion of multiple bodies in potential flow. These idealized models, although lacking in biological realism, may provide valuable insight into the fluid's role in the coordinated motion of fish schools. Natural fish schools seem to consist of two opposing but balanced behaviours: a desire to avoid collisions within the group and a desire to stay close to the group, see, e.g., Hoare *et al.* (2001) and Shaw (1975). It is clear why an individual fish wants to avoid collisions. But why do fish seem to have this basic urge for joining a group? Biologists explain this as an evolutionary behaviour resulting from several factors such as protection from predators, profiting from a larger search pattern in the quest for food, and advantages for social and mating activities, Shaw (1970). From the energy point of view, it is widely believed that fish exploit the vortices in the wake of other fish of the group to reduce their locomotory costs, which is consistent with the recent findings in Liao *et al.* (2003). We emphasize that the goal of this work is not to present biologically accurate models of fish schooling but rather to develop simple models with idealized fluid motion that provide insight into the role of the hydrodynamic coupling in the motion of multiple submerged bodies. In § 5 of this work, we study the fluid's role in collision avoidance and motion coordination of multiple bodies and provide evidence that a free body coordinates its motion with that of its neighbours even in the absence of shed vortices. We tie our work to the classical work of Lamb (1932) by first considering the example of two submerged cylinders where one is forced into periodic oscillations and analysing the response of the free cylinder to this parametric excitation. Note that the interactions of two bodies in potential flow was also considered in the recent works of Burton, Gratus & Tucker (2004), Wang (2004) and Crowdy, Surana & Yick (2007).

The organization of this paper is as follows. In § 2, the Lagrangian function of the solid–fluid system is expressed in terms of the solid variables only. The equations of motion are derived for the problem of two submerged cylinders in § 3. One cylinder is forced into periodic oscillations and the response of the second cylinder to this parametric excitation is analysed. A separation of time scales in the response of the free cylinder is performed in § 4. In § 5, the role of the fluid in collision avoidance and motion coordination is examined numerically through examples. We summarize the findings of this work in § 6.

2. Formulation of the dynamics

Consider N planar rigid solids immersed in an infinitely large volume of an inviscid incompressible fluid which is at rest at infinity. Assume that the fluid particles may slip along the boundaries of the solid but cavities are not allowed to form in the fluid nor at the interface. That is, the normal components of the solid and fluid velocities are equal at the interface. Further, assume that the motion of the solid remains planar at all time and does not generate vorticity in the fluid, that is, starting with zero circulation (irrotational flow), the flow remains irrotational at all times. In this case, the dynamics of the solid–fluid system can be described in terms of the solid

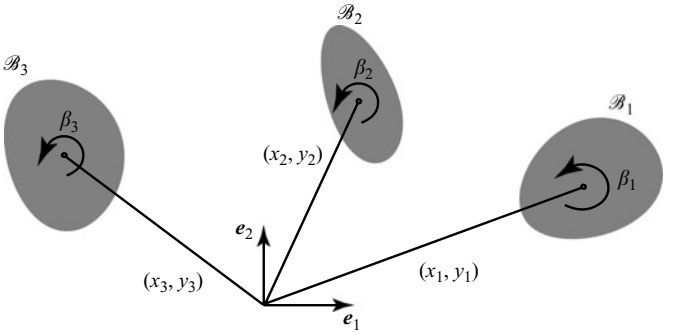

FIGURE 1. Solid bodies of arbitrary shape are placed in an infinite two-dimensional domain of incompressible irrotational fluid. The plane is horizontal (no gravity) and the solids are assumed to be neutrally buoyant.

variables only without explicitly incorporating the ambient fluid, as outlined in this section.

It is convenient for studying the motion of the submerged solids to introduce an orthonormal inertial frame $\{\boldsymbol{e}_{1,2,3}\}$ where $\{\boldsymbol{e}_1, \boldsymbol{e}_2\}$ span the plane of motion and $\boldsymbol{e}_3$ is the unit normal to this plane. The configuration of each solid $\mathscr{B}_i$, $i = 1, \ldots, N$, can then be described by a rotation β_i about $\boldsymbol{e}_3$ and a translation (x_i, y_i) in the $\{\boldsymbol{e}_1, \boldsymbol{e}_2\}$ directions, as shown in figure 1. Further, let $\Omega_i = \dot{\beta}_i$ and $v_i = (\dot{x}_i, \dot{y}_i)$ be, respectively, the angular and translational velocities of $\mathscr{B}_i$ expressed relative to a frame attached to $\mathscr{B}_i$. For conciseness, the velocity of $\mathscr{B}_i$ will be denoted by the column vector ξ_i where $\xi_i = (\Omega_i, v_i)^T$.

The kinetic energy T of the solid–fluid system can be written as the sum of the energies of the solids $T_{\mathscr{B}_i}$ and the energy of the fluid $T_{\mathscr{F}}$; namely,

$$T = \sum_{i=1}^{N} T_{\mathscr{B}_i} + T_{\mathscr{F}}. \tag{2.1}$$

The kinetic energy $T_{\mathscr{B}_i}$ can be written in the form

$$T_{\mathscr{B}_i} = \tfrac{1}{2}\, \xi_i^T \mathbb{I}_i^s \xi_i, \qquad i = 1, 2 \ldots, N. \tag{2.2}$$

Here, $\mathbb{I}_i^s$ is a 3×3 diagonal matrix with diagonal entries (I_i, m_i, m_i) where I_i is the moment of inertia of $\mathscr{B}_i$ and m_i its mass. It is important to recall that the solid bodies are neutrally buoyant, that is, $\rho_s = \rho_f$.

The kinetic energy of the fluid $T_{\mathscr{F}}$ is given by

$$T_{\mathscr{F}} = \frac{1}{2} \int_{\mathscr{F}} \rho_f |u|^2 \, \mathrm{d}a, \tag{2.3}$$

where u is the spatial velocity field of the fluid and $\mathrm{d}a$ is the standard area element on $\mathbb{R}^2$. For potential flow, the fluid velocity can be written as the gradient of a potential function $u = \nabla\phi$, where the potential ϕ is the solution to Laplace's equation

$$\Delta\phi = 0 \tag{2.4}$$

subject to the boundary conditions

$$\left.\begin{array}{ll} \nabla\phi \cdot n_i = (v_i + \Omega_i \times X_i) \cdot n_i & \text{on } \partial\mathscr{B}_i, \\ \nabla\phi = 0 & \text{at } \infty. \end{array}\right\} \tag{2.5}$$

Here, n_i is the outward unit normal to the boundary $\partial\mathscr{B}_i$ and X_i is the position vector of a point on $\partial\mathscr{B}_i$ relative to the respective mass centre. By linearity of Laplace's equation (using the principle of superposition), one can write, following Kirchhoff,

$$\phi = \sum_{i=1}^{N} (\Omega_i \cdot \chi_i + v_i \cdot \varphi_i), \tag{2.6}$$

where χ_i and $\varphi_i = (\varphi_i^x, \varphi_i^y)$ are called velocity potentials and are solutions to Laplace's equation subject to Neumann-type boundary conditions at their interface with the solid bodies; namely

$$\nabla\chi_i \cdot n_i = (\boldsymbol{e}_3 \times X_i) \cdot n_i \quad \text{on } \partial\mathscr{B}_i, \qquad \nabla\chi_i \cdot n_j = 0 \quad \text{on } \partial\mathscr{B}_j, \ j \neq i, \tag{2.7}$$

and (similar conditions hold for φ_i^y)

$$\nabla\varphi_i^x \cdot n_i = \boldsymbol{e}_1 \cdot n_i \quad \text{on } \partial\mathscr{B}_i, \qquad \nabla\varphi_i^x \cdot n_j = 0 \quad \text{on } \partial\mathscr{B}_j, \ j \neq i. \tag{2.8}$$

It should be clear from (2.7)–(2.8) that χ_i, φ_i^x and φ_i^y depend not only on the shape of $\mathscr{B}_i$ but also on that of the other submerged bodies and their relative positions with respect to $\mathscr{B}_i$.

Using $u = \nabla\phi$ where ϕ is written as in (2.6) and following a standard procedure (see, e.g., Kanso *et al.* 2005) to show that $T_{\mathscr{F}}$ of (2.3) can be rewritten as

$$T_{\mathscr{F}} = \sum_{i=1}^{N} \sum_{j=1}^{N} \frac{1}{2} \xi_i^T \, \mathbb{I}_{ij}^f \, \xi_j. \tag{2.9}$$

The 3×3 *added-inertia* matrices $\mathbb{I}_{ij}^f$ depend on the geometry and relative configurations of the submerged solids and are of the form

$$\mathbb{I}_{ij}^f = \left(\begin{array}{c|c} J_{ij} & d_{ij}^T \\ \hline d_{ij} & M_{ij} \end{array} \right), \tag{2.10}$$

where J_{ij} are scalars that represent added moments of inertia due to the presence of the fluid,

$$J_{ij} = -\rho_f \int_{\partial\mathscr{B}_j} \chi_i \frac{\partial\chi_j}{\partial n} \, \mathrm{d}s, \tag{2.11}$$

M_{ij} are 2×2 symmetric matrices that represent added masses,

$$M_{ij} = \begin{pmatrix} -\rho_f \displaystyle\int_{\partial\mathscr{B}_j} \varphi_i^x \frac{\partial\varphi_j^x}{\partial n} \, \mathrm{d}s & -\rho_f \displaystyle\int_{\partial\mathscr{B}_j} \varphi_i^x \frac{\partial\varphi_j^y}{\partial n} \, \mathrm{d}s \\ -\rho_f \displaystyle\int_{\partial\mathscr{B}_j} \varphi_i^y \frac{\partial\varphi_j^x}{\partial n} \, \mathrm{d}s & -\rho_f \displaystyle\int_{\partial\mathscr{B}_j} \varphi_i^y \frac{\partial\varphi_j^y}{\partial n} \, \mathrm{d}s \end{pmatrix}, \tag{2.12}$$

and d_{ij} are 2×1 arrays that reflect a coupling between the angular and translational motions due to the hydrodynamic effects,

$$d_{ij} = \begin{pmatrix} -\frac{1}{2}\rho_f \left(\displaystyle\int_{\partial\mathscr{B}_j} \varphi_i^x \frac{\partial\chi_j}{\partial n} \, \mathrm{d}s + \int_{\partial\mathscr{B}_j} \chi_i \frac{\partial\varphi_j^x}{\partial n} \, \mathrm{d}s \right) \\ -\frac{1}{2}\rho_f \left(\displaystyle\int_{\partial\mathscr{B}_j} \varphi_i^y \frac{\partial\chi_j}{\partial n} \, \mathrm{d}s + \int_{\partial\mathscr{B}_j} \chi_i \frac{\partial\varphi_j^y}{\partial n} \, \mathrm{d}s \right) \end{pmatrix}. \tag{2.13}$$

Note that ds is a line (e.g. arclength) element. It should be clear from the above expressions that each added-inertia matrix $\mathbb{I}_{ij}^f$ is symmetric and, hence, has three independent principal axes. Further, $\mathbb{I}_{ij}^f = \mathbb{I}_{ji}^f$. This symmetry reflects a reciprocity in the effects two submerged solids $\mathscr{B}_i$ and $\mathscr{B}_j$ have on each other due to the hydrodynamic coupling.

The total kinetic energy T in (2.1) can be rewritten by virtue of (2.2) and (2.9) as

$$T = \sum_{i=1}^{N} \sum_{j=1}^{N} \frac{1}{2} \xi_i^T \, \mathbb{I}_{ij} \, \xi_j, \tag{2.14}$$

where $\mathbb{I}_{ii} = \mathbb{I}_i^s + \mathbb{I}_{ii}^f$ and $\mathbb{I}_{ij} = \mathbb{I}_{ij}^f$ for $i \neq j$. Note that, although there is an analogy between $\mathbb{I}_i^s$ and $\mathbb{I}_{ij}^f$, they are fundamentally distinct. For example, in translation, unlike the body's actual mass, the added mass depends on the direction of the motion.

For the neutrally buoyant rigid bodies, the Lagrangian function L of the solid–fluid system is equal to the kinetic energy T given in (2.14). Clearly, L is a function of the solid variables only (both position and velocity). The same holds for the equations of motion which can be derived from Hamilton's variational principle (or the Lagrange–d'Alembert variational principle in the presence of applied external forces and moments), which requires that

$$\delta \int_{t_0}^{t_f} L \, \mathrm{d}t = 0 \tag{2.15}$$

for all variations that vanish at the end points t_0 and t_f. In the following sections, we derive the equations of motion for a number of systems and discuss their behaviour and relevance to understanding the role of hydrodynamic coupling in motion coordination.

3. Two submerged cylinders and Lamb's example

We consider the problem of two cylinders in potential flow where one is forced to oscillate along the line joining the two centres while the second responds freely due to hydrodynamic coupling. This problem is inspired by a similar example of two submerged spheres considered in Lamb (1932). Lamb concluded, using approximate potentials and an averaging analysis, that the free sphere is "on average" attracted towards the oscillating body. In this section, we study, both analytically and numerically, the two-dimentional analogue (we consider two cylinders instead of two spheres) and show that *the free cylinder can be either repelled away or attracted towards the oscillating body depending on the phase of oscillation.* We also indicate that this conclusion is true for the example of the two spheres considered by Lamb, while his analysis only captures the attracting behaviour.

The two submerged cylinders (of radii a and b respectively) are constrained to move along the line joining their centres, which is chosen to coincide with the $\boldsymbol{e}_1$-direction, and the centre of $\mathscr{B}_1$ is placed initially at the origin, as shown in figure 2. Following the notation in § 2, the coordinates of the centres of the cylinders are labelled as $(x_1, 0)$ and $(x_2, 0)$, respectively. The Lagrangian governing this (one-dimensional) motion of the system is given by

$$L = \tfrac{1}{2}\left(M_{11}\dot{x}_1^2 + 2M_{12}\dot{x}_1\dot{x}_2 + M_{22}\dot{x}_2^2\right), \tag{3.1}$$

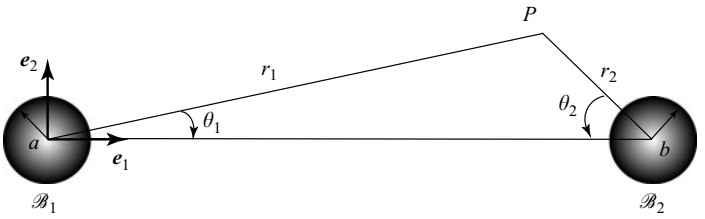

FIGURE 2. Lamb's example: two spherical bodies in potential flow where $\mathscr{B}_1$ is forced to oscillate along the line joining the two centres and $\mathscr{B}_2$ responds freely. In this section, we consider the analogous case of two submerged cylinders.

where M_{11}, M_{12} and M_{22} are given by (2.12); namely

$$M_{11} = -\rho_f \int_0^{2\pi} \varphi_1 \frac{\partial \varphi_1}{\partial n} a \, \mathrm{d}\theta_1, \quad M_{12} = -\rho_f \int_0^{2\pi} \varphi_1 \frac{\partial \varphi_2}{\partial n} b \, \mathrm{d}\theta_2,$$
$$M_{22} = -\rho_f \int_0^{2\pi} \varphi_2 \frac{\partial \varphi_2}{\partial n} b \, \mathrm{d}\theta_2, \tag{3.2}$$

where φ_1 and φ_2 are solutions to Laplace's equations subject to the Neumann boundary conditions in (2.8). The potential function of the surrounding fluid is $\phi = \varphi_1 \dot{x}_1 + \varphi_2 \dot{x}_2$. Note that, for notational convenience, we dropped the superscript x from φ_1^x and φ_2^x in (2.8) since the motion is constrained to be in the x-direction only.

Now, let $\mathscr{B}_1$ oscillate about the origin, that is, assume that $x_1 = f(t)$ is a prescribed periodic function of time. The response of $\mathscr{B}_2$ to this *parametric excitation* is governed by the Euler–Lagrange equation

$$\frac{\mathrm{d}}{\mathrm{d}t}(M_{12}\, \dot{f} + M_{22}\, \dot{x}_2) - \frac{1}{2}\left(\frac{\partial M_{11}}{\partial x_2} \dot{f}^2 + 2 \frac{\partial M_{12}}{\partial x_2} \dot{f} \dot{x}_2 + \frac{\partial M_{22}}{\partial x_2} \dot{x}_2^2 \right) = 0. \tag{3.3}$$

This is a scalar second-order differential equation whose solution $x_2(t)$ gives the dynamic response of $\mathscr{B}_2$ to the prescribed parametric excitation $f(t)$. The added masses M_{11}, M_{12} and M_{22} are typically functions of the distance between the two cylinders (i.e. depend on x_2 in a non-trivial way) and need to be computed in order to study the dynamic response of $\mathscr{B}_2$. We present two methods: a numerical solution based on a panel method and an analytical approximation following the approach in Lamb (1932), assuming the distance between the cylinders is large compared to their radii.

3.1. *Computing the added masses using a panel method*

We compute the added masses in (3.2) by solving for the velocity potentials φ_i $(i = 1, 2)$ using a standard panel method. As discussed in § 2, φ_i are the solutions of Laplace's equation $\Delta \varphi_i = 0$, subject to Neumann-type boundary conditions (2.8) at the interface with the solid bodies, which in this example gives

$$\nabla \varphi_i \cdot \boldsymbol{n}_i = \cos\theta_i \quad \text{on } \partial \mathscr{B}_i, \qquad \nabla \varphi_i \cdot \boldsymbol{n}_j = 0 \quad \text{on } \partial \mathscr{B}_j, \quad j \neq i. \tag{3.4}$$

The problem of solving Laplace's equation for φ_1 and φ_2 over the fluid domain $\mathscr{F}$ subject to (3.4) can be replaced by an easier boundary value problem which is then solved numerically using a boundary element method. The theoretical foundation of such methods is based on reformulating Laplace's equations as a boundary integral equation, using the divergence theorem (see, e.g., Moran 1984). As a result, only the boundary surfaces of the submerged bodies need to be discretized, hence the

computational advantages of such methods. We use the method devised by Hess & Smith (1966) which utilizes a piecewise-constant distribution of source singularities over the surfaces of the submerged bodies and computes this distribution as the solution of an integral equation (see Kanso *et al.* 2005 for more details). Physically, this *fictitious* source distribution induces a velocity field in the fluid that is equivalent to the velocity field resulting from the motion of the submerged bodies.

In this example, we solve for two distinct source distributions corresponding the two sets of boundary conditions in (3.4). The velocity potential functions φ_1 and φ_2 are now obtained at the discretized boundaries $\partial\mathscr{B}_1$ and $\partial\mathscr{B}_2$, and the added masses in (3.2) are then computed. Finally, note that in the case of N submerged bodies undergoing general translations and rotations, one needs to solve for $3\times N$ source distributions corresponding to boundary conditions (2.7)–(2.8) on χ_i, φ_i^x and φ_i^y, as done for the examples examined in § 5.

3.2. *Analytic approximation of the added masses*

We derive approximate expressions for M_{ij} in (3.2) based on approximate velocity potentials φ_1 and φ_2, assuming the distance between the bodies is large compared to their radii.

We first compute an approximate expression for φ_1. The velocity potential due to a unit velocity of $\mathscr{B}_1$ in the $\boldsymbol{e}_1$-direction in the absence of $\mathscr{B}_2$ would be

$$\varphi = \frac{a^2}{r_1}\cos\theta_1, \tag{3.5}$$

where (r_1, θ_1) denote the polar coordinates relative to the centre of $\mathscr{B}_1$. We use this potential function as a first approximation to φ_1, which corresponds to a unit velocity of $\mathscr{B}_1$ in the $\boldsymbol{e}_1$-direction while $\mathscr{B}_2$ is at rest. But (3.5) does not take into consideration the presence of $\mathscr{B}_2$ and gives rise to a non-zero normal velocity on $\partial\mathscr{B}_2$ which can be cancelled by setting $\varphi_1 = \varphi + \tilde{\varphi}$, where $\tilde{\varphi}$ is to be determined. To this end, evaluate φ in the neighbourhood of $\mathscr{B}_2$ in terms of (r_2, θ_2), the polar coordinates relative to the centre of $\mathscr{B}_2$, to obtain

$$\varphi = \frac{a^2}{r_1^2}\, r_1\cos\theta_1 = \frac{a^2}{r_1^2}(r_{12} - r_2\cos\theta_2) \approx \frac{a^2}{r_{12}^2}(r_{12} - r_2\cos\theta_2), \tag{3.6}$$

where $r_{12} = r_1\cos\theta_1 + r_2\cos\theta_2$ is the distance between the centres of $\mathscr{B}_1$ and $\mathscr{B}_2$ and is assumed to be large relative to a and b, see figure 2. One can readily check that the non-zero normal velocity induced by φ on $\partial\mathscr{B}_2$ can be cancelled using a term of the form

$$\tilde{\varphi} = -\frac{a^2b^2}{r_{12}^2}\frac{\cos\theta_2}{r_2}. \tag{3.7}$$

Now, the resulting expression for $\varphi_1 = \varphi + \tilde{\varphi}$ when evaluated on the surface of $\mathscr{B}_1$ adds an extra term to the normal velocity at $\partial\mathscr{B}_1$, i.e. it is no longer only due to a unit velocity of $\mathscr{B}_1$ in the $\boldsymbol{e}_1$-direction. To fix this, we repeat the same procedure. We first evaluate $\tilde{\varphi}$ in the neighbourhood of $\mathscr{B}_1$ in terms of r_1 and θ_1 to obtain

$$\tilde{\varphi} = -\frac{a^2b^2}{r_{12}^4}(r_{12} - r_1\cos\theta_1), \tag{3.8}$$

where, as before, we used $r_1\cos\theta_1 + r_2\cos\theta_2 = r_{12}$ and $r_{12} \gg a, b$. Then, to cancel the additional component induced by $\tilde{\varphi}$ on the normal velocity at $\partial\mathscr{B}_1$, we need an

additional term of the form

$$\tilde{\tilde{\varphi}} = \frac{a^4 b^2}{r_{12}^4} \frac{\cos\theta_1}{r_1}. \tag{3.9}$$

This process can be continued further to obtain more accurate expressions for the velocity potential. We stop the approximation at this stage and use $\varphi_1 = \varphi + \tilde{\varphi} + \tilde{\tilde{\varphi}}$, which can be evaluated at $\partial\mathscr{B}_1$ and $\partial\mathscr{B}_2$ as follows:

$$\varphi_1|_{\partial\mathscr{B}_1} = a\cos\theta_1 + \frac{2a^3b^2\cos\theta_1}{r_{12}^4} - \frac{a^2b^2}{r_{12}^3}, \quad \varphi_1|_{\partial\mathscr{B}_2} = \frac{a^2}{r_{12}} - \frac{2a^2 b\cos\theta_2}{r_{12}^2}. \tag{3.10}$$

Similarly, an approximate expression for φ_2 is given by

$$\varphi_2|_{\partial\mathscr{B}_2} = b\cos\theta_1 + \frac{2b^3a^2\cos\theta_1}{r_{12}^4} - \frac{b^2a^2}{r_{12}^3}, \quad \varphi_2|_{\partial\mathscr{B}_1} = \frac{b^2}{r_{12}} - \frac{2b^2 a\cos\theta_2}{r_{12}^2}. \tag{3.11}$$

The approximate values of φ_1 and φ_2 in (3.10)–(3.11) are used to calculate the added mass in (3.2):

$$M_{11} = \rho\pi a^2\left(1 + \frac{2a^2b^2}{r_{12}^4}\right), \quad M_{12} = -2\rho\pi\frac{a^2b^2}{r_{12}^2}, \quad M_{22} = \rho\pi b^2\left(1 + \frac{2a^2b^2}{r_{12}^4}\right). \tag{3.12}$$

These expressions can be further simplified if we retain only terms up to order $1/r_{12}^2$, which leads to

$$M_{11} = \rho\pi a^2, \quad M_{12} = -2\rho\pi\frac{a^2b^2}{r_{12}^2}, \quad M_{22} = \rho\pi b^2. \tag{3.13}$$

3.3. *Dynamic response of the free body*

This section studies the dynamic response of $\mathscr{B}_2$ to prescribed oscillations $f(t)$ of $\mathscr{B}_1$ and compares the behaviour of $\mathscr{B}_2$ based on the the added masses computed in § 3.1 to that based on the approximate added masses derived in § 3.2. For the remaining part of this paper, we assume SI units for all physical quantities.

We assume that the cylinders have zero inertias in vacuum and the same radius a with $2a^2 = 1\,\mathrm{m}^2$, and set the fluid density to be $\rho_f = 1/\pi\ \mathrm{kg\,m^{-3}}$. We calculate the added masses M_{ij}, $(i, j = 1, 2)$, as described in § 3.1. The values of the added masses are then substituted into (3.3) and a standard, variable-time-step, fourth- to fifth-order Runge–Kutta integration scheme is used to solve for $x_2(t)$. Note that the derivatives $\partial M_{ij}/\partial x_2$ are computed numerically using the following rule:

$$\frac{\partial M_{ij}}{\partial x_2} \approx \frac{1}{12h}(M_{ij}(x_2 - 2\delta) - 8M_{ij}(x_2 - \delta) + 8M_{ij}(x_2 + \delta) - M_{ij}(x_2 + 2\delta)) \tag{3.14}$$

where δ is an arbitrary small variation in x_2 (chosen to be $\delta = 0.01/3$ m in the numerical scheme). In figure 3, $\mathscr{B}_2$ is shown to drift away from $\mathscr{B}_1$ when the latter is forced to oscillate at $f(t) = \sin(t)$ whereas $\mathscr{B}_2$ is attracted towards $\mathscr{B}_1$ for $f(t) = -\sin(t)$.

In the case of approximate added masses, we have from (3.13) that M_{11} and M_{22} are constants while M_{12} is function of the distance $r_{12} = x_2 - f$. Employing this in (3.3) yields the following analytical equation:

$$M_{22}\,\ddot{x}_2 + M_{12}\,\ddot{f} - \frac{\partial M_{12}}{\partial x_2}\dot{f}^2 = 0. \tag{3.15}$$

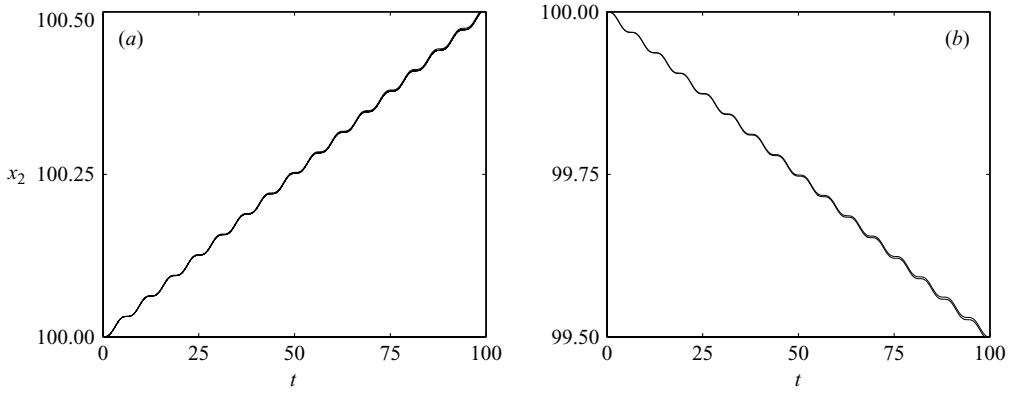

FIGURE 3. The response of $\mathscr{B}_2$ to forced oscillations of $\mathscr{B}_1$. Initially, $\mathscr{B}_1$ and $\mathscr{B}_2$ are placed at $x_1(0) = 0$ m and $x_2(0) = 100$ m respectively. (*a*) $x_2(t)$ versus t due to $\mathscr{B}_1$ oscillations of the form $x_1(t) = f(t) = -\sin(t)$. The free body $\mathscr{B}_2$ drifts away from the oscillating body. (*b*) $x_1(t) = f(t) = \sin(t)$, and $\mathscr{B}_2$ is attracted towards $\mathscr{B}_1$. In both plots, two solutions are shown, which are in excellent agreement. One solution is obtained by computing the added mass using a panel method, and the other is based on approximate expressions for the added mass.

Then, substitute the values of M_{11}, M_{12} and M_{22} from (3.13) into the above equation to obtain

$$\ddot{x}_2 = \frac{2a^2}{(x_2 - f)^2}\ddot{f} + \frac{4a^2}{(x_2 - f)^3}\dot{f}^2. \tag{3.16}$$

Note that this equation is valid for $(x_2 - f) \gg a$. Hence, a positive scaling parameter ϵ is introduced to reflect the magnitude of the radius a relative to the large distance $x_2 - f$ between the two cylinders. The amplitude of the prescribed oscillation of $\mathscr{B}_1$ is chosen to be of order ϵ. To this end, use ϵf instead of f in (3.16) and again use $2a^2 = 1$ m^2 to obtain

$$\ddot{x}_2 = \frac{\epsilon\ddot{f}}{(x_2 - \epsilon f)^2} + \frac{2\epsilon^2\dot{f}^2}{(x_2 - \epsilon f)^3}. \tag{3.17}$$

We solve (3.17) for $x_2(t)$ using the same integration scheme. Figure 3 shows that the response of $\mathscr{B}_2$ is consistent with that based on computing the added masses for the two types of excitation $f(t) = \pm\sin(t)$. Body $\mathscr{B}_2$ is attracted towards $\mathscr{B}_1$ when $f(t) = \sin(t)$ and $\mathscr{B}_2$ is repelled away from $\mathscr{B}_1$ when $f(t) = -\sin(t)$. However, $\mathscr{B}_2$ drifts away from $\mathscr{B}_1$ for $f(t) = \pm\sin^n(t)$ for > 1, irrespective of the sign, see figure 4, depictis which the response when $n = 2, 3$. Notice that, in figures 3 and 4, the response of $\mathscr{B}_2$ consists of a slow drift (towards or away from $\mathscr{B}_1$) and superimposed rapid oscillations.

Note that the direction of motion depends on the phase of the forcing in the case when $f(t) = \pm\sin(t)$ whereas the motion direction remains unchanged when $f(t) = \pm\sin^n(t)$ with $n > 1$. This behaviour can be interpreted physically as follows: in order to determine the direction of motion of the free cylinder, it is not enough to know the distance between the two cylinders and the frequency of oscillation, one must also go back in time to find the initial velocity of the forced cylinder. When the forced cylinder has a non-zero initial velocity, it instantaneously imparts

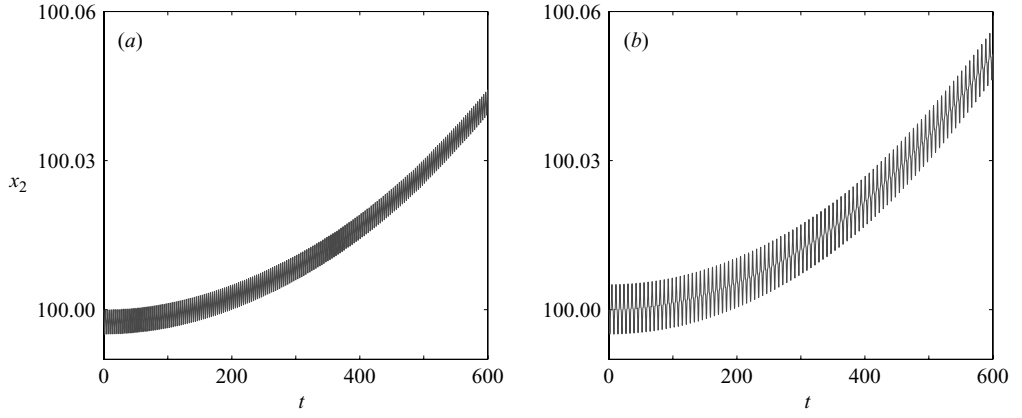

FIGURE 4. The response of $\mathscr{B}_2$ to forced oscillations of $\mathscr{B}_1$. Here, $\mathscr{B}_2$ is initially placed at $x_2(0) = 100$ m and the solution $x_2(t)$ is based on approximate expressions of the added mass. (*a*) $x_2(t)$ versus t for $\mathscr{B}_1$ oscillating at $f(t) = \sin^2(t)$, and in (*b*) $f(t) = \sin^3(t)$. Interestingly, the free body drifts away from the forced body in a quadratic manner for $f(t) = \sin^n(t)$ when $n > 1$, as discussed further in the multiple-scales analysis in § 4.

an initial non-zero impulse to the fluid† which biases the direction of motion of the free cylinder. The initial impulse of the fluid is equal and opposite to the initial momentum of the forced body, that is, the fluid initial impulse is $-m_1 \dot{f}(0)$ (starting from rest, the total impulse of the solid–fluid system at time $t = 0$ is zero). When $f(t) = \sin(t)$, the initial fluid impulse is $-m_1 < 0$ which biases the motion of the free body towards the forced body, and vice versa when $f(t) = -\sin(t)$. Also, when $f(t) = \pm \sin^n(t)$, the initial fluid impulse is zero and has no effect on the direction of motion of the free body, whose intrinsic response is to drift away from the forced body. This interpretation is consistent with the numerical observations in figures 3 and 4 as well as the results of the multiple-scales analysis of § 4. Indeed, note that, when $f(t) = \pm \sin t$, equations (4.9) and (4.10) describing the slow response can be rewritten as $x_{2\epsilon} = A - (\dot{f}(0)/A^2)\tau + \cdots$ (A is the initial separation distance and τ is the slow time scale), which, to leading order, decreases when $\dot{f}(0)$ is positive and increases when $\dot{f}(0)$ is negative.

4. Multiple-scale analysis of the two-cylinder example

In this section, (3.17) is decomposed into components that are evolving at two distinct time scales: a rapid time t of $O(1)$ defined by the frequency of the prescribed oscillations of $\mathscr{B}_1$ and a slow time $\tau = \epsilon t$ of $O(\epsilon)$ defined by the drift rate of $\mathscr{B}_2$.

In multiple-scales analysis, the dynamic variable is typically written as a polynomial expansion in ϵ

$$x_{2\epsilon}(t) = x_{20}(t, \tau) + \epsilon x_{21}(t, \tau) + \epsilon^2 x_{22}(t, \tau) + \cdots, \tag{4.1}$$

which can be expressed in the form (see the Appendix for details)

$$x_{2\epsilon}(t) = A + A_0(\tau) + \epsilon(A_1(\tau) + B_0(t)) + \epsilon^2(A_2(\tau) + B_1(t)) + \cdots. \tag{4.2}$$

† The impulse of the fluid is a momentum-like quantity. The fluid momentum in its strict definition is infinite since the volume of the fluid is infinite.

The time derivatives can be expressed as

$$\frac{\mathrm{d}}{\mathrm{d}t} = \frac{\partial}{\partial t} + \epsilon \frac{\partial}{\partial \tau}, \quad \frac{\mathrm{d}^2}{\mathrm{d}t^2} = \frac{\partial^2}{\partial t^2} + 2\epsilon \frac{\partial^2}{\partial t \partial \tau} + \epsilon^2 \frac{\partial^2}{\partial \tau^2}. \tag{4.3}$$

Relations (4.3) are substituted into (4.2) and terms of the same order in ϵ are collected to give

$$\dot{x}_{2\epsilon}(t) = \dot{A} + \epsilon(A_0' + \dot{B}_0) + \epsilon^2(A_1' + \dot{B}_1) + \cdots, \quad \ddot{x}_{2\epsilon}(t) = \ddot{A} + \epsilon \ddot{B}_0 + \epsilon^2(A_0'' + \ddot{B}_1) + \cdots, \tag{4.4}$$

where the prime denotes the derivative relative to slow time τ, and the over dot denotes the derivative relative to t.

To write a series expansion of the right-hand side of (3.17) in terms of ϵ, we need the following result: given a series $y = y_0 + \epsilon y_1 + \epsilon^2 y_2 + \cdots$, one has

$$\frac{1}{y^n} = \frac{1}{y_0^n}\left(1 - \epsilon n \frac{y_1}{y_0} + \epsilon^2 \left(\frac{n(n+1)}{2}\frac{y_1^2}{y_0^2} - n\frac{y_2}{y_0}\right) + \cdots\right). \tag{4.5}$$

Now, substitute (4.2) into the right-hand side of (3.17) and use the result in (4.5) to obtain a polynomial expansion in terms of ϵ. Then, substitute (4.4) into the left-hand side of (3.17) and collect terms of the same order on both sides. One obtains, when truncating the expansion (4.1) at $O(\epsilon^2)$, that is, for $x_{2\epsilon} = x_{20} + \epsilon x_{21} = A(t) + A_0(\tau) + \epsilon B_0(t)$,

$$O(1): \quad \ddot{A} = 0, \tag{4.6a}$$

$$O(\epsilon): \quad \ddot{B}_0 = \frac{\ddot{f}}{(A + A_0)^2}, \tag{4.6b}$$

$$O(\epsilon^2): \quad A_0'' = \frac{2\dot{f}^2 + 2\ddot{f} f - 2\ddot{f} B_0}{(A + A_0)^3}. \tag{4.6c}$$

At the leading order, the solution $A(t)$ corresponds to $\epsilon = 0$ which, starting at rest, is a constant function equal to the initial position of $\mathscr{B}_2$, i.e. $A = x_2(0)$ when $\dot{x}_2(0) = 0$. The remaining two equations in (4.6*a*) are used to solve for $A_0(\tau)$ and $B_0(t)$. Note that the initial conditions $x_2(0) = A$ and $\dot{x}_2(0) = 0$ translate to initial conditions for $A_0(\tau)$ and $B_0(t)$ using $x_{2\epsilon} = A + A_0(\tau) + \epsilon B_0(t)$ and $\dot{x}_{2\epsilon} = \epsilon A_0' + \epsilon \dot{B}_0$ as follows:

$$x_{2\epsilon}(0) = A \implies A_0(0) = B_0(0) = 0, \quad \dot{x}_{2\epsilon}(0) = 0 \implies A_0'(0) = -\dot{B}_0(0). \tag{4.7}$$

We now solve for $A_0(\tau)$ and $B_0(t)$ in the case when $\mathscr{B}_1$ is forced to oscillate as a sinusoidal function of time $f(t) = \sin^n(t)$, where n is a positive integer. In this case, the solution to (4.6*b*) is of the form

$$B_0(t) = \frac{f(t)}{(A + A_0)^2} + \left(\underbrace{\dot{B}_0(0) - \frac{\dot{f}(0)}{(A + A_0(0))^2}}_{=0}\right) t + B_0(0) = \frac{\sin^n(t)}{(A + A_0)^2}, \tag{4.8}$$

where $B_0(0) = 0$ from (4.7) and we set the linear term to zero to obtain a periodic response $B_0(t)$ in the fast time scale t. We distinguish two cases based on the value of n.

Case of $n = 1$. One has:

$$\dot{B}_0(0) - \frac{\dot{f}(0)}{(A + A_0(0))^2} = 0 \implies \dot{B}_0(0) = \frac{1}{A^2},$$

and, using (4.7), obtains $A_0'(0) = -\dot{B}_0(0) = -1/A^2$. Now, the Taylor expansion for $A_0(\tau)$ about $\tau = 0$ is given by

$$A_0(\tau) = A_0(0) + A_0'(0)\tau + \cdots \implies A_0(\tau) = -\frac{1}{A^2}\tau + \cdots,$$

and, correspondingly,

$$x_{2\epsilon}(t) = A - \frac{1}{A^2}\tau + \epsilon\frac{\sin(t)}{(A + A_0)^2} + \cdots. \tag{4.9}$$

The above equation means that, when $\mathscr{B}_1$ is forced to oscillate as $\sin(t)$, although at $t = 0$ $\mathscr{B}_1$ moves towards $\mathscr{B}_2$, the free body $\mathscr{B}_2$ is attracted towards the forced body. Now, if $\mathscr{B}_1$ is forced as $-\sin(t)$, i.e. if the phase of the oscillation is changed by π, then

$$x_{2\epsilon}(t) = A + \frac{1}{A^2}\tau - \epsilon\frac{\sin(t)}{(A + A_0)^2} + \cdots, \tag{4.10}$$

and $\mathscr{B}_2$ is repelled away from the oscillating body. In both scenarios, the linear slow-time behaviour and the superimposed fast-time-scale oscillations are consistent with the response obtained by direct numerical integration shown in figure 3.

Case of $n > 1$. One has $\dot{f}(0) = 0$ which yields using (4.7) and (4.8) that $A_0'(0) = -\dot{B}_0(0) = 0$. Therefore, we should consider the quadratic term in τ to understand the slow-time response $A_0(\tau)$ which is governed by (4.6*c*). Using the value of $B_0(t)$ from (4.8), (4.6*c*) becomes

$$A_0'' = \frac{2\dot{f}^2 + 2\ddot{f}f}{(A + A_0)^3} - \frac{2\ddot{f}f}{(A + A_0)^5}. \tag{4.11}$$

We average out the fast oscillations on the right-hand side and consider the average behaviour of A_0, denoted by $\langle A_0\rangle$. To this end, for $f(t) = \pm\sin^n(t)$, the average of $f\ddot{f}$ over a 2π period is zero, and the average of (4.11) over a period of rapid oscillation yields

$$\langle A_0\rangle'' = \frac{2\langle\dot{f}^2\rangle}{(A + \langle A_0\rangle)^3}, \tag{4.12}$$

where $\langle\dot{f}^2\rangle$ is positive. Clearly, $\langle A_0\rangle$ increases with a leading term that is quadratic in τ. That is, the free body is repelled away from $\mathscr{B}_1$ for $f(t) = \pm\sin^n(t)$. This result is consistent with the direct numerical integration shown in figure 4.

Remarks on Lamb's analysis. We conclude this section by returning to Lamb's example of two submerged spheres where one is forced to oscillate periodically while the second responds freely. One can readily verify, following the notation and procedure employed in § 3, that the response of sphere $\mathscr{B}_2$ is dictated by

$$\ddot{x}_2 = \frac{\epsilon\ddot{f}}{2(x_2 - \epsilon f)^3} - \frac{3\epsilon^2\dot{f}^2}{2(x_2 - \epsilon f)^4}, \tag{4.13}$$

where the radius a of the sphere is taken to be $3a^3 = 1\,\mathrm{m}^3$. Lamb (1932) derived a similar equation and concluded, using an averaging approach, that the free sphere drifts towards the forced one. His analysis fails to capture the case when the sphere drifts away because, when he took the average of both sides of (4.13), he treated the terms given by $(x_2 - \epsilon f)$ as constant.

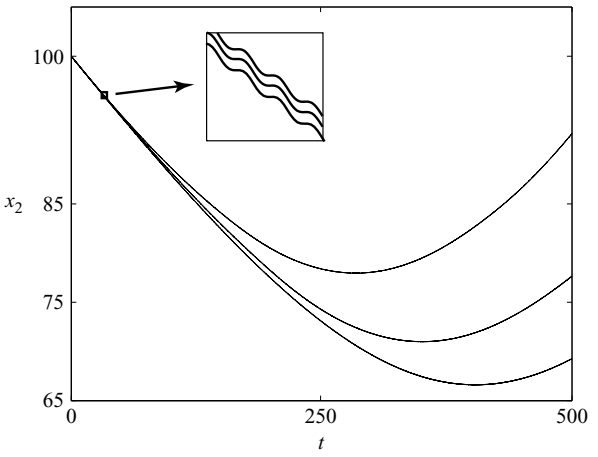

FIGURE 5. The response $x_2(t)$ of $\mathscr{B}_2$ due to $x_1(t) = f(t) = \sin(25t)$. Clearly, $\mathscr{B}_2$ is initially attracted towards $\mathscr{B}_1$, reaches a minimum separation distance then drifts away. When $\mathscr{B}_2$ goes back to its initial position, it now has a non-zero velocity in the positive x_1-direction and continues to drift away without turning back. The lowermost line corresponds to the simulation using the panel method in § 3.1 while the middle and upper lines are based on the approximate added masses in (3.12) and (3.13), respectively. The solution based on approximate potentials is expected to be less accurate when the distance between the two bodies decreases. Indeed, the exact and approximate solutions diverge as time increases but their qualitative behaviour is consistent.

5. Fluid's role in collision avoidance and motion coordination

We examine the role of hydrodynamic coupling further through a number of examples, and show that this coupling could help in collision avoidance and motion coordination. This result may be relevant to understanding the coordinated motion in fish schooling.

5.1. *Collision avoidance*

The fluid seems to act as a collision avoidance mechanism in the two-cylinder example discussed above. Figure 5 is a depiction of the time response of $\mathscr{B}_2$ due to forced oscillations $f(t) = \sin(25t)$ which shows that $\mathscr{B}_2$ moves towards the oscillating body, reaches a minimum separation distance, then starts to drift away. We did several numerical experiments by integrating (3.17) with forcing of the form $f(t) = K\sin(\omega t)$ to try to understand what exactly determines the minimum separation distance. In the first set of experiments, we varied the frequency ω while letting the amplitude $K = 1$ and the initial velocity of the free body $\dot{x}_2(0) = 0$. We found that the minimum separation distance does not change significantly as a function of the frequency but the time it takes to reach the minimum separation distance decreases as ω increases. We obtained similar results when we fixed $\omega = 25$ and varied the amplitude of the forcing. In the third set of experiments, we held $K = 1$ and $\omega = 25$ and varied the initial velocity of the free body. The minimum separation distance decreased when we gave the free body an initial velocity towards the oscillating body.

These results can be interpreted as follows. One could associate an impulse with the slow drift that is proportional to the drift velocity. Now, the drift towards the oscillating body is a transient behaviour dictated by the initial impulse imparted to the fluid and by the impulse associated with the slow drift. The body reverses its direction of motion when the impulse associated with the slow drift balances the initial impulse

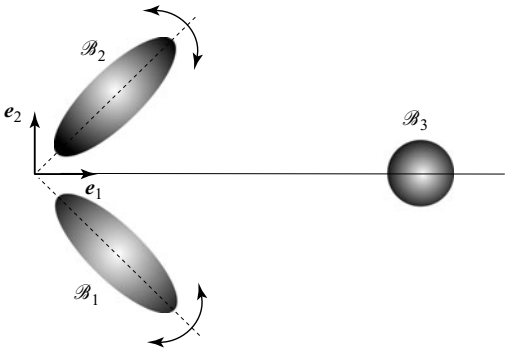

FIGURE 6. A two-link mechanism is forced to oscillate about its hinge joint placed at the origin while a circular body $\mathscr{B}_3$ is free to respond, through the hydrodynamic coupling, to this *parametric excitation*. The response of $\mathscr{B}_3$ for chosen parameters is depicted in figure 7.

imparted to the fluid. As we increase the amplitude or frequency of the forcing, not only the initial impulse imparted to the fluid increases but also the impulse associated with the slow drift increases correspondingly. As a result, the time it takes to overcome the initial impulse decreases while the minimum separation distance is not significantly affected. Now, when we fix the amplitude and frequency of the forcing and assign a non-zero initial velocity to the free body, we change the initial impulse without affecting the impulse associated with the slow drift. As a result, both the minimum separation distance and the time it takes to reach that distance change. In particular, the minimum separation distance decreases when the free body is given an initial velocity towards the oscillating body. In order to rigorously prove or disprove these statements, one could use the method of multiple scales described in § 4 to obtain estimates of the velocity and impulse associated with the slow drift. One may need to include higher-order terms in the multiple-scales expansions to better approximate the slow drift. Such detailed analysis is beyond the scope of the present paper.

A similar behaviour is observed in the example shown in figure 6 where two identical bodies $\mathscr{B}_1$ and $\mathscr{B}_2$ are used to form a two-link mechanism with a hinge joint placed at the origin while a free circular body $\mathscr{B}_3$ is initially placed at $(x_3(0), 0)$. The two links $\mathscr{B}_1$ and $\mathscr{B}_2$ are forced to oscillate about their common joint according to $\beta_1(t) = \beta_1(0) + f(t)$ and $\beta_2(t) = -\beta_1(t)$, where $f(t)$ is periodic in t. That is, the motion of the mass centres of the two links is given by $x_i(t) = l\cos\beta_i(t)$ and $y_i(t) = l\sin\beta_i(t)$, $(i = 1, 2)$, where l is the constant distance from the joint to the mass centres. The velocities $\xi_{1,2}$ corresponding to the prescribed motion are given by $\xi_{1,2}^T = (\pm\dot{f}, \mp l\dot{f}\sin f, \pm l\dot{f}\cos f)$, where the upper sign is associated with ξ_1.

The Lagrangian function of the system in figure 6 is given by (2.14) with $N = 3$. The equations governing the motion of $\mathscr{B}_3$ are obtained by substituting (2.14) in Hamilton's principle (2.15) subject to variations in the orientation β_3 and position (x_3, y_3) of $\mathscr{B}_3$. However, due to the geometric symmetry of the bodies and the symmetry in the forcing of $\mathscr{B}_1$ and $\mathscr{B}_2$, one needs to take variations with respect to x_3 only. This yields a differential equation of the form

$$\frac{\mathrm{d}}{\mathrm{d}t}\left[(0,1,0)\left(\mathbb{I}_{31}^f\xi_1 + \mathbb{I}_{32}^f\xi_2 + \mathbb{I}_{33}\xi_3\right)\right] = \frac{\partial L}{\partial x_3}, \tag{5.1}$$

whose solution $x_3(t)$ is the motion of $\mathscr{B}_3$ in the $\mathbf{e}_1$-direction. The added masses involved in (5.1) are computed as discussed in § 3.1 and their derivatives with respect

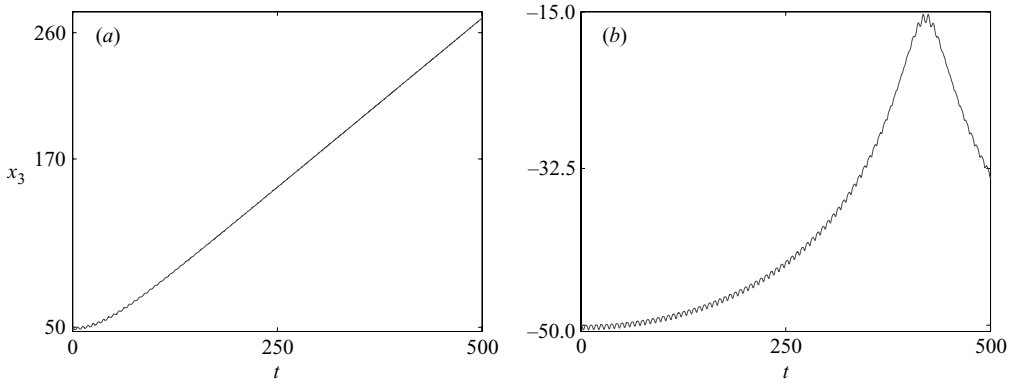

FIGURE 7. The response $x_3(t)$ of $\mathscr{B}_3$ to oscillations $f(t) = (\pi/8)(1 - \cos t)$ rad. (*a*) $x_3(0) = 50\,\mathrm{m}$ and (*b*) $x_3(0) = -50\,\mathrm{m}$. In (*a*), $\mathscr{B}_3$ drifts away from the oscillating two-link mechanism, and in (*b*), $\mathscr{B}_3$ drifts towards the oscillating two-link mechanism, reaches a minimum separation distance, then starts to drift away.

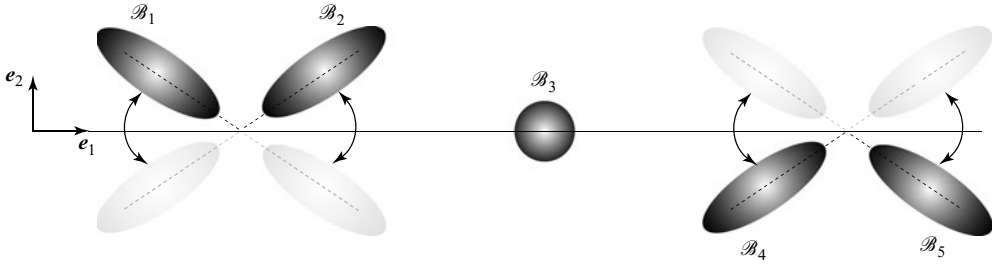

FIGURE 8. The two-link rigid bodies are forced to oscillate about their respective hinge joints and to translate in the $\mathbf{e}_1$-direction while a circular body $\mathscr{B}_3$ is free to respond, through the hydrodynamic-coupling, to this *parametric excitation*. The coordinated response of $\mathscr{B}_3$ to prescribed motion of the outer two bodies is depicted in figure 9.

to x_3 are calculated numerically analogously to (3.14). For the numerical integration, the radius of $\mathscr{B}_3$ is set equal to 3 m, while the major and minor axes of the ellipses $\mathscr{B}_1$ and $\mathscr{B}_2$ are chosen to be 10 and 3 m, respectively. Figure 7 shows the response of $\mathscr{B}_3$ to oscillations $\beta_1(t) = -\beta_2(t) = \pi/4 + \pi/8(1 - \cos t)$ rad. In plot (*a*), $x_3(0) = 50\,\mathrm{m}$ and $\mathscr{B}_3$ drifts away from the oscillating two-link mechanism. Plot (*b*) corresponds to $x_3(0) = -50\,\mathrm{m}$. Here, $\mathscr{B}_3$ drifts towards the two-link body, reaches a minimum separation distance, then starts to drift away.

One may think of this example as a simple model of an aquatic animal, say a scallop or a jellyfish, that is trying to feed by opening and closing its mouth. It seems that the two-link animal fails to attract the food, i.e. $\mathscr{B}_3$, by merely undergoing oscillatory movement *in potential flow* in the absence of a mechanism for vortex shedding. Alternatively, one could think of the oscillating two-link body as a simple model of a flapping fish. The numerical result in figure 7 suggests that the flapping motion may play a role, through the hydrodynamic coupling, in keeping a minimum distance of separation between the fish and its neighbour. This idea is explored further in the example in § 5.2.

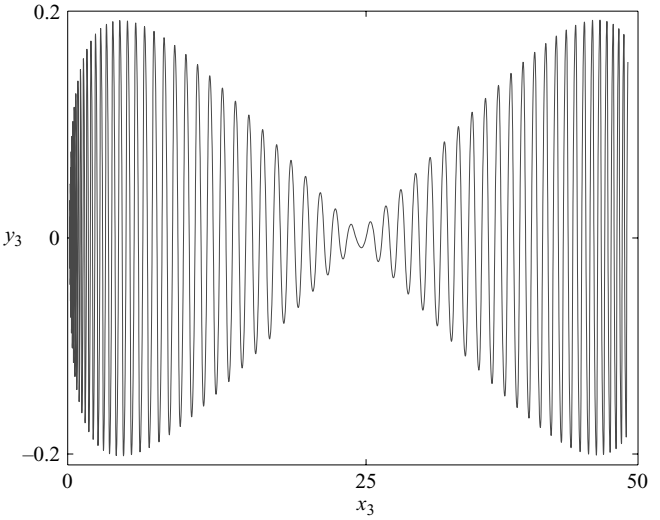

FIGURE 9. The motion of $\mathscr{B}_3$ in the (x, y)-plane in response to prescribed flapping $f(t) = (\pi/8)\sin(t)$ rad and translation $x(t)$ with onstant velocity of the outer two-link bodies. Clearly, $\mathscr{B}_3$ moves in the $\mathbf{e}_1$-direction and its response is coordinated with the motion of its neighbours.

5.2. *Motion coordination*

Consider the example shown in figure 8 of two identical articulated bodies, each made of two rigid links, and a free circular body $\mathscr{B}_3$ initially placed at mid-distance between the two mechanisms. The articulated bodies are initially placed such that their major axis lies along the $\mathbf{e}_1$-direction. Further, they are forced to oscillate about their respective joints such that their oscillatory motion is out of phase, more specifically, $\beta_1(t) = \beta_5(t) = f(t)$ while $\beta_2(t) = \beta_4(t) = -f(t)$. The articulated bodies are also forced into a translational motion $x(t)$ along the $\mathbf{e}_1$-direction. To this end, the motion of the mass centres of the individual links is given by $x_i(t) = x(t) + l\cos\beta_i(t)$ and $y_i(t) = l\sin\beta_i(t)$ $(i = 1, 2, 4, 5)$, where l is defined as in the previous example. The velocities $\xi_1 (= \xi_5)$ and $\xi_2 (= \xi_4)$ are given by $\xi_{1,2}^T = (\pm\dot{f}, x(t) \mp l\dot{f}\sin f, \pm l\dot{f}\cos f)$, where the upper signs are associated with ξ_1.

The equations governing the motion of $\mathscr{B}_3$ are obtained by substituting the Lagrangian (2.14) in Hamilton's principle (2.15) subject to variations in the orientation β_3 and position (x_3, y_3) of $\mathscr{B}_3$. However, due to the geometric symmetry of $\mathscr{B}_3$, one needs to take variations with respect to x_3 and y_3 only. This yields the following differential equations:

$$\frac{\mathrm{d}}{\mathrm{dt}}\left[\begin{pmatrix}0 & 1 & 0\\ 0 & 0 & 1\end{pmatrix}\left(\mathbb{I}_{31}^f\xi_1 + \mathbb{I}_{32}^f\xi_2 + \mathbb{I}_{34}^f\xi_4 + \mathbb{I}_{35}^f\xi_5 + \mathbb{I}_{33}\xi_3\right)\right] = \begin{bmatrix}\dfrac{\partial L}{\partial x_3}\\ \dfrac{\partial L}{\partial y_3}\end{bmatrix}. \tag{5.2}$$

These equations can be integrated numerically following the procedure described in § 5.1. The major and minor axes of the ellipses are chosen to be 10 m and 5 m, respectively, while the radius of $\mathscr{B}_3$ is equal to 3 m. The initial distance from the centre of $\mathscr{B}_3$ to the joint of the two-link bodies is taken to be 80 m. Figure 9 depicts the response of $\mathscr{B}_3$ to the case when the outer two-link bodies are oscillating with $f(t) = (\pi/8)\sin(t)$ rad and translating in the $\mathbf{e}_1$-direction with velocity equal

to $0.1\,\mathrm{m\,s^{-1}}$. Clearly, the response of $\mathscr{B}_3$ is coordinated with the motion of its neighbours. The two-link bodies may be thought of as simple models of flapping fish. The coordinated response of $\mathscr{B}_3$ to the motion of the outer two bodies suggests that the hydrodynamic coupling may play an essential role in the coordinated motion of fish schools. Further investigations will be undertaken to understand the persistency and stability of such coordinated motions over a range of geometries and parameters values.

6. Summary

This paper considered the dynamics of a finite number of rigid solids moving in potential flow. The dynamics of the solid–fluid system was formulated in terms of the solid variables only using Kirchhoff potentials. The problem of two submerged bodies where one is forced into periodic oscillations was analysed. It was observed that the hydrodynamic coupling causes the free body to drift away from or towards the oscillating body. The method of multiple scales was used to separate the slow drift from the fast response. Interestingly, the free body, when attracted towards the forced one, starts to drift away after it reaches certain separation distance, which suggests that the hydrodynamic coupling may help in preventing collision. The fluid's role in collision avoidance and motion coordination was examined further through a number of examples. In particular, it was shown that a free body can coordinate its motion with that of its neighbour's through the hydrodynamic coupling. This result may be relevant to understanding the coordinated motion in fish schooling.

The authors would like to thank Professors Paul Newton, Jerrold E. Marsden and Andrew J. Szeri for useful comments and discussions. E. K.'s work is partially supported by the National Science Foundation through the award CMMI 06-44925.

Appendix. An alternative form of the multiple-scales expansion

Claim. *In perturbation theory, the dynamic response x due to an external excitation of order ϵ is typically written as a polynomial expansion in ϵ, see e.g. Nayfeh (1973). In the case of multiple time scales, say when x evolves at two distinct time scales – a fast time t and a slow time $\tau = \epsilon t$ – the expansion is written as follows:*

$$x_\epsilon(t) = x_0(t,\tau) + \epsilon x_1(t,\tau) + \epsilon^2 x_2(t,\tau) + \cdots = \sum_{r=0}^{\infty} \epsilon^r x_r(t,\tau). \tag{A 1}$$

We claim that this series can be equivalently written in the form

$$x_\epsilon(t) = A(t) + \sum_{i=0}^{\infty} \epsilon^i (A_i(\tau) + \epsilon B_i(t)) \tag{A 2}$$

where $A(t)$ is the solution corresponding to $\epsilon = 0$, and $A_i(0) = 0$ for all i.

Remark. One of the main advantages of using (A 2) over (A 1) in § 4 is the absense of cross-coupling terms that depend on both t and τ. In particular, one obtains $\partial^2/\partial t\,\partial\tau = 0$.

Proof. A term $x_r(t,\tau)$ in (A 1) is expanded as a Taylor series in t and τ as follows:

$$x_r(t,\tau) = x_{r0} + \sum_{i=1}^{\infty}\sum_{n=0}^{i} x_{r,i,n}\, t^n\, \tau^{i-n} = x_{r0} + \sum_{i=1}^{\infty} x_{r,i,0}\, \tau^i + \sum_{i=1}^{\infty}\sum_{n=1}^{i} x_{r,i,n}\, t^n\, \tau^{i-n} \tag{A 3}$$

where we have seperated the term corresponding to $n=0$. Use $t^n\,\tau^{i-n} = t^n\,(\epsilon t)^{i-n} = t^i\,\epsilon^{i-n}$ in (A 3) to obtain

$$x_r(t,\tau) = x_{r0} + \sum_{i=1}^{\infty} x_{r,i,0}\,\tau^i + \sum_{i=1}^{\infty} t^i \sum_{n=1}^{i} x_{r,i,n}\,\epsilon^{i-n} = x_{r0} + \sum_{i=1}^{\infty} x_{r,i,0}\,\tau^i + \sum_{i=1}^{\infty} t^i \sum_{n=0}^{i-1} x_{r,i,n}\,\epsilon^n. \tag{A 4}$$

Now, interchange the order of summation in the last term of (A 4),

$$x_r(t,\tau) = x_{r0} + \sum_{i=1}^{\infty} x_{r,i,0}\tau^i + \sum_{i=0}^{\infty} \epsilon^i \sum_{n=i+1}^{\infty} x_{r,i,n}\,t^n, \tag{A 5}$$

and define the functions $A_r(\tau)$, $\tilde{B}_{r0}(t)$ and $\tilde{B}_{ri}(t)$ (for $i>0$) as follows:

$$A_r(\epsilon t) = \sum_{i=1}^{\infty} x_{r,i,0}\,\tau^i, \quad \tilde{B}_{r0}(t) = x_{r0} + \sum_{n=1}^{\infty} x_{r,i,n}\,t^n, \quad \tilde{B}_{ri}(t) = \sum_{n=i+1}^{\infty} x_{r,i,n}\,t^n. \tag{A 6}$$

Note that, by definition, $A_r(0)=0$ for all r and $\epsilon^i \tilde{B}_{ri}(t)$ is independent of τ and powers of τ. Substitute (A 6) in (A 5), then use the resulting form for $x_r(t,\tau)$ in (A 1) to obtain

$$x_\epsilon(t) = \sum_{r=0}^{\infty} \epsilon^r\, x_r(t,\tau) = \sum_{r=0}^{\infty} \epsilon^r A_r(\tau) + \sum_{r=0}^{\infty}\sum_{i=0}^{\infty} \epsilon^{r+i} \tilde{B}_{ri}(t)\ . \tag{A 7}$$

Collect powers of ϵ^r in the second term of (A 7) to obtain

$$x_\epsilon(t) = \tilde{B}_{00}(t) + \sum_{r=0}^{\infty} \epsilon^r A_r(\tau) + \sum_{r=1}^{\infty} \epsilon^r \sum_{i+j=r} \tilde{B}_{ij}(t). \tag{A 8}$$

Now, define

$$A(t) = \tilde{B}_{00}(t), \quad \tilde{B}_r = \sum_{i+j=r} \tilde{B}_{ij}(t)\ . \tag{A 9}$$

Replacing (A 9) in (A 8) yields $x_\epsilon(t) = A(t) + \sum_{r=0}^{\infty} \epsilon^r A_r(\tau) + \sum_{r=1}^{\infty} \epsilon^r \tilde{B}_r(t)$. Finally, introduce $B_r = \tilde{B}_{r+1}$ to obtain

$$x_\epsilon(t) = A(t) + \sum_{r=0}^{\infty} \epsilon^r (A_r(\tau) + \epsilon B_r(t)). \tag{A 10}$$

Note that for $\epsilon = 0$, one has $x_0(t) = A(t)$ since $A_r(0) = 0$ for all r by construction. That is, $A(t)$ is the solution for $\epsilon = 0$. Therefore, (A 1) is equivalent to (A 2) and our claim is proved. □

REFERENCES

Burton, D. A., Gratus, J. & Tucker, R. W. 2004 Hydrodynamic forces on two moving discs. *Theor. Appl. Mech.* **31**, 153–188.

Childress, S. 1981 *Mechanics of Swimming and Flying*. Cambridge University Press.

Crowdy, D., Surana, A. & Yick, K.-Y. 2007 The irrotational flow generated by two planar stirrers in inviscid fluid. *Phys. Fluids* **19**, 018103.

Hess, J. L. & Smith, A. M. O. 1966 Calculation of potential flow about arbitrary bodies. *Prog. Aeronaut. Sci.* **8**, 1–139.

Hoare, D., Ward, A. J., Couzin, I. D., Croft, D. & Krause, J. 2001 A grid-net technique for the analysis of fish positions in free-ranging fish schools. *J. Fish Biol.* **59**, 1667–1672.

Kanso, E. & Marsden, J. E. 2005 Optimal motion of an articulated body in a perfect fluid. *44th IEEE Conference on Decision and Control*, vol. 44, pp. 2511– 2516.

Kanso, E., Marsden, J. E., Rowley, C. W. & Melli-Huber, J. 2005 Locomotion of articulated bodies in a perfect fluid. *J. Nonlinear Sci.* **15**, 255–289.

Kelly, S. D. 1998 The mechanics and control of robotic locomotion with applications to aquatic vehicles. PhD thesis, California Institute of Technology.

Lamb, H. 1932 *Hydrodynamics*, 6th Edn. Dover.

Liao, J. C., Beal, D. N., Lauder, G. V. & Triantafyllou, M. S. 2003 Fish exploiting vortices decrease muscle activity. *Science* 302, 1566–1569.

Lighthill, M. J. 1975 *Mathematical Biofluiddynamics*. Society for Industrial and Applied Mathematics, PA.

Moran, J. 1984 *An Introduction to Theoretical and Computational Aerodynamics*. John Wiley & Sons.

Müller, U. K. 2003 Fish'n Flag. *Science* **302**, 1511–1512.

Nayfeh, A. H. 1973 *Perturbation Methods*. Wiley-Interscience.

Radford, J. 2003 Symmetry, reduction and swimming in a perfect fluid. PhD thesis, California Institute of Technology.

Shaw, E. 1975 Fish in schools. *Natural History* **84** (8), 40–46.

Shaw, E. 1970 Schooling in fishes: critique and review. In *Development and Evolution of Behavior*, pp. 452–480. W. H. Freeman and Company, San Francisco.

Taylor, G. I. 1952 Analysis of the swimming of long and narrow animals. *Proc. R. Soc. Lond.* A **214**, 158–183.

Wang, Q. X. 2004 Interaction of two circular cylinders in inviscid fluid. *Phys. Fluids* **16**, 4412–4425.

Webb, P. W. 1991 Composition and mechanics of routine swimming of rainbow trout *Oncorhynchus mykiss*. *Can. J. Fish. Aquat. Sci.* **48**, 583–590.

Wu, T. Y. 1971 Hydrodynamics of swimming fish and cetaceans. *Adv. Appl. Maths* **11**, 1–63.